

WATER CONSTITUENT RETRIEVAL AND LITTORAL BOTTOM MAPPING USING HYPERSPECTRAL APEX IMAGERY AND SUBMERSED ARTIFICIAL SURFACES

Sebastian Rößler, Patrick Wolf, Thomas Schneider, Stefan Zimmermann, and Arnulf Melzer

Technische Universität München, Limnological Institute, 82393 Iffeldorf, Germany;
Email: [sebastian.roessler\(at\)mytum.de](mailto:sebastian.roessler@mytum.de)

ABSTRACT

The analysis of littoral bottom properties such as bathymetry and coverage (i.e. plant identification) often requires knowledge about the composition of relevant optically active water constituents like phytoplankton, suspended particulate matter and coloured dissolved organic matter, which influence the radiative transfer in water due to scattering and/or absorption. These inherent optical properties (IOPs) of the water column can be retrieved in optically deep water (i.e., with no reflectance contribution of the bottom) by using physically based inversion techniques. In shallow water – which often differs from deep water in the amount of water constituents due to terrestrial input from the shore – a reliable estimation of IOPs requires at least a valid bottom reflectance, which is difficult to measure in water. An accurate estimation of water constituents is essential to the retrieval of bottom reflectance and subsequent identification of invasive aquatic plants, which was the main goal of this project.

In an experimental approach, the application of artificial surfaces for retrieving water constituents as well as bottom depth was tested during the hyperspectral APEX campaign 2011 covering Lake Starnberg in southern Germany. Two silo foils (10 metres wide and 50 metres long) were spread on the littoral bottom covering depths from 0.5 to 16 metres and acting as a very bright (white side of the foil) as well as a very dark (black side of the foil) reflective bottom albedo for the ENVI add-on BOMBER in terms of water constituents retrieval and bottom depth estimation. Reflectance spectra of the foils are known from laboratory measurements. *In situ* measurements were performed in water using RAMSES spectrometers and processed using the algorithms implemented in BOMBER as well as the inversion software WASI. The results show best performance for the black sided foil regarding pixel unmixing, water constituent retrieval and depth estimation, which agreed well with the WASI inversion results of the downwelling irradiance, which was used for validation due to lacking bottom influence.

INTRODUCTION

In water remote sensing applications focussing on shallow littoral areas a large reflectance contribution originates from the water column itself. The inherent optical properties (IOPs) of the water column depend on the concentrations of the optically active constituents namely phytoplankton (CHL), suspended particulate matter (SPM) and coloured dissolved organic matter (cDOM) (1). They influence the radiative transfer in water due to scattering and absorption of incident radiation. Depending on the illumination conditions, they can be related to apparent optical properties (AOPs) such as the vertical attenuation coefficient and the reflection of optically deep water. Several parameterizations exist for relating IOPs to AOPs (2-6) for optically deep water. For shallow water, additionally the depth and the bottom albedo have to be taken into account.

Although water constituent retrieval approaches are mainly focussed on marine environments using multispectral sensors enabling a large coverage like SeaWiFS (7), CZCS (8), MODIS (9,10), MERIS (9) and ETM+ (9,11), several algorithms have been adapted to be used on inland water bodies as well. A review of spaceborne remote sensing studies focussing on water constituents is given by Odermatt et al. (12). The application of hyperspectral airborne remote sensing for water quality in inland waters has also been shown in several studies (13-15). Inland water applications

in shallow water areas either focus on the retrieval of water constituents (16-19) or on the retrieval of bottom properties like vegetation coverage (20-23) or bathymetry (24).

One main issue with the application of physically based modelling of IOPs from shallow water like WASI (25), MIP (20) and BOMBER (26) is a reliable bottom albedo that is used as a reference for depth and constituent retrieval. In this study, the application of artificial bottom albedo of very bright and dark surfaces was tested to evaluate the retrieval of water constituents and depth using the bio-optical software BOMBER (26). A similar study has already been carried out by Tolk et al. (27) using a tank with black and white bottom for different SPM concentrations. According to their findings, the wavelength range between 740 and 900 nm is least affected by the bottom due to strong absorption of the water itself and thus the remaining scattering results from SPM and not from the bottom. Another tank experiment with dark and bright surfaces (and constant water constituents) was used to correct *in situ* measured vegetation reflectance (28).

In our approach, a combination of artificial dark and white surfaces (silo foils) in a natural environment (lake shore) and intensive spectroradiometric *in situ* measurements were performed simultaneously with a hyperspectral APEX flight. Through this a large data set was acquired covering the same targets (foils) with known reflectance behaviour which was processed further using WASI and BOMBER and compared with regard to uncertainties of water constituent retrieval and depth estimation.

STUDY SITE

Lake Starnberg (47°55'N, 11°19'E) in southern Bavaria occupies an area of 65 km² and is Germany's fifth largest lake (Figure 1). Its expansion is 20 km, its maximum width 4.7 km. The lake was formed by the Isar-Loisach glacier during the last glacial period (29) and has an average depth of 53.2 metres (maximum 127.8 metres).

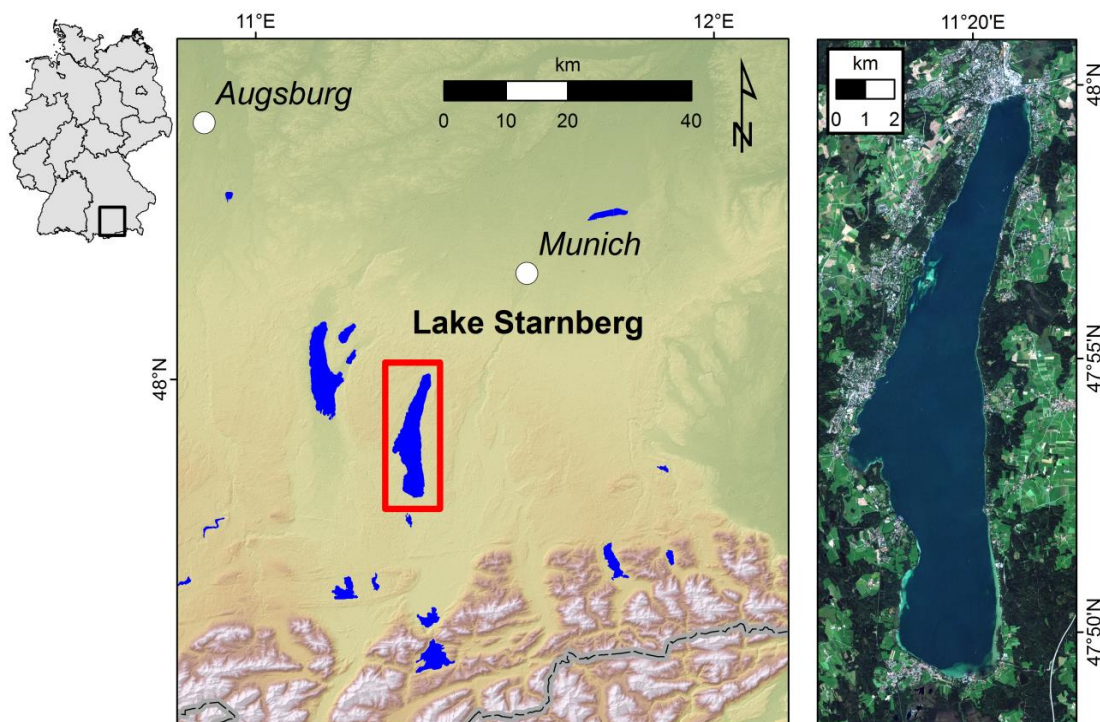


Figure 1: Location of Lake Starnberg and RGB composite of a RapidEye scene from 03/09/11.

Large shallow littoral terraces are mainly located at the western lakeside and were therefore chosen for *in situ* measurements as well as guiding the orientation of the flight lines during the APEX campaign 2011. At this lakeside, several areas are covered by submersed aquatic macrophytes such as *Potamogeton pectinatus*, *Potamogeton perfoliatus*, *Chara* spp., *Najas marina* and *Elodea nuttallii*. The last two are considered to be invasive plants since increasing water temperatures

promote their expansion. The identification of these two species was the main purpose of this study leading to the hypothesis that they can be recognized if artificial surfaces with known reflectances are classified correctly. The main test site near the village of Bernried was chosen due to high abundance of *Najas marina* at depths between 2 and 6 metres. Submersed foils were spread out here to gather information about IOPs from shallow water areas. In this oligotrophic lake, concentrations of phytoplankton were reported to be between 2 and 5 µg/l in winter and 6-12 µg/l in summer, respectively (21).

MATERIAL AND METHODS

BOMBER

BOMBER (Bio-Optical Model Based tool for Estimating water quality and bottom properties from Remote sensing images) is an ENVI add-on that was recently published by Giardino et al. (26). It relies on the model by Lee et al. (30,31) which has been developed with HYDROLIGHT (1) simulations and can be used for optically deep water (i.e. with no influence of the bottom) and shallow water. The deep water mode only requires water leaving reflectance and simplified spectral response functions (Gaussian functions built from central wavelength and FWHM value). In shallow water mode, the underwater sun zenith angle θ_w has to be provided as well as three different bottom reflectances ρ for linear bottom unmixing. For the shallow water model, a contribution of the water reflectance itself (depending on the IOPs, left term of Eq. 1), as well as the bottom contribution (right side of Eq. 1) depending on the water depth H are calculated according to Eq. 1 (30):

$$r_{rs} = r_{rs}^{\infty} \left(1 - A_0 \exp \left[- (K_d + K_u^C) H \right] \right) + A_1 \rho \exp \left[- (K_d + K_u^B) H \right] \quad (1)$$

The variables A_0 and A_1 are weighting factors for the contributions of water and bottom to the apparent reflectance (5,30). The parameterization of the attenuation for the downwelling irradiance (K_d) and upwelling radiance from the bottom (K_u^B) and from the water (K_u^C) was adapted from Lee et al. (31) based on HYDROLIGHT simulations and can be changed in BOMBER. They relate the IOPs total absorption (a) and total backscattering (b_b) to the AOPs attenuation (K) and deep water reflection (r_{rs}^{∞}) through Eq. 2 to Eq. 5:

$$K_d = \frac{a + b_b}{\cos \theta_w} \quad (2)$$

$$K_u^C = \left[1.03 \left(1 + 2.4 \frac{b_b}{a + b_b} \right)^{0.5} \right] (a + b_b) \quad (3)$$

$$K_u^B = \left[1.04 \left(1 + 5.4 \frac{b_b}{a + b_b} \right)^{0.5} \right] (a + b_b) \quad (4)$$

$$r_{rs}^{\infty} = \left(0.084 + 0.17 \frac{b_b}{a + b_b} \right) \frac{b_b}{a + b_b} \quad (5)$$

θ_w is the sun zenith angle under water, a the sum of individual absorption coefficients (CHL, SPM, cDOM and water) and b_b the sum of backscattering coefficients (CHL, SPM and water). Eqs. (3) to (5) already include the parameterizations of Lee et al. (1999) (31). In BOMBER, a least square optimization is performed to minimize the error (err) between measured (R_{rs}) and modelled reflectance (\hat{R}_{rs}) above water for all wavelengths λ under examination (Eq. 6):

$$err = \sqrt{\sum_{\lambda_{min}}^{\lambda_{max}} (R_{rs}(\lambda) - \hat{R}_{rs}(\lambda))^2} \quad (6)$$

Simulated data

The performance of BOMBER on APEX data was tested using a simulated data set. For three different surfaces (white foil, black foil and bare sediment), 30 reflectance spectra were randomly created from a large range of water constituent concentrations (CHL: 1-5 $\mu\text{g/l}$; SPM: 1-5 mg/l ; cDOM: 0.2-0.7 m^{-1}) and depths (0.5-16 metres) for each bottom coverage. The radiative transfer equation of Lee et al. (30,31) – which is also the physical basis of BOMBER – was used for forward modelling. The spectra were further resampled to the spectral resolution of APEX.

The simulated reflectance spectra were subsequently inverted using a python (version 2.7) routine which comprises the equations of BOMBER. In contrast to the forward modelling, the inversion has to be performed on a lower spectral resolution and three endmembers (white foil, black foil and bare sediment) were provided for bottom unmixing. The bottom reflectance spectra for these surfaces, as well as the two plant reflectances (*Najas marina*, *Chara* spp.) used for the final classification of the whole image, are shown in Figure 2.

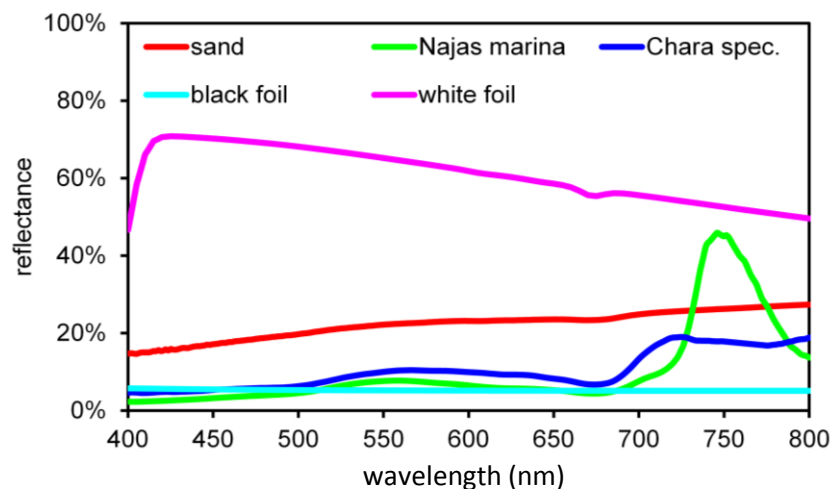


Figure 2: Bottom reflectance of possible endmembers for spectral unmixing.

The inversion of the simulated data set was performed to find out whether the three different surfaces were assigned to the right endmember by calculating the classification accuracy (percentage of pixel with 100% coverage of the right endmember). In addition, the accurate determination of depth and water constituents was evaluated by calculating the root-mean-square error (*RMSE*), the mean absolute percentage error (*MAPE*) and the coefficient of determination (R^2) between input values and BOMBER-derived output values (separately for each bottom coverage).

Field data set

Field work during the APEX image data acquisition included bringing out the two foils with the aid of scientific divers as well as spectral measurements. The location for the foils was guided by morphometric aspects. To cover a littoral area with a large range of depths, sites were selected to provide very shallow depths (0.5 m) for the first 20 metres of the total length as well as very deep (>15 m) areas where the reflected signal by the bottom can be neglected. Additionally, the foils were placed at a distance of 50 m from each other to assure comparable quantities of water constituents and avoid overframing of the black foil by the white one. The black foil has an average reflectance of 5% (Figure 2) so that the apparent reflectance above the water surface clearly differs from the reflectance of optically deep water. However, it can be used to minimize the effect of the bottom due to a missing wavelength dependency and a generally low reflectance.

Spectral *in situ* measurements were performed using three submersible RAMSES spectroradiometers (TriOS). Two hemispherical sensors (ACC) measured the downwelling (E_d) and upwelling irradiance (E_u) and one radiance sensor (ARC) the upwelling radiance (L_u) with a field of view of 7° . The sensors were triggered simultaneously and enabled the irradiance reflectance ($R = E_u/E_d$), remote sensing reflectance ($R_{rs} = L_u/E_d$) and anisotropy ($Q = E_u/L_u$) to be calculated.

Remote sensing ground truth data were collected directly above the foils at four different depths (0.5, 3, 5, 8 m). At each measuring point, in-water measurements were collected at 1 m depth intervals (11 iterations) ranging from just above the foils ($R(b)$) to just below the water surface ($R(0-)$). Above-water measurements ($R(0+)$) were also recorded to be compared with APEX data. A total of 522 individual measurements were made.

Applying BOMBER and WASI to *in situ* measurements

The bio-optical model BOMBER has also been applied to the *in situ* measured intensities of L_u and E_d to retrieve water constituents and bottom properties (depth, coverage). For inversion it has to be taken into account that the measurements were made in water and that the entrance optics of the sensors were not aligned at the same depth level to avoid instrument shadowing. The intensity of E_d has to be lowered by 0.475 m to correspond to the depth level of the L_u and E_u sensors. To account for this difference, a python routine was created where the sensors measuring L_u and E_d are treated separately and the depth difference between them is taken into account. For the least square optimization, the L_u measurements were chosen as target functions to derive water constituents and bottom properties. Eq. (1) was modified according to our requirements (separating L_u and E_d). Therefore, the radiance at a given depth (z_1) is separated into a part originating from the water column (L_u^C) and a bottom contribution (L_u^B) (Eq. 7):

$$L_u(z_1) = L_u^C(z_1) + L_u^B(z_1) \quad (7)$$

To account for the depth difference between z_1 and z_2 , the intensity of $E_d(z_1)$ has to be lowered using the attenuation coefficient K_d (Eq. 8):

$$E_d(z_1) = E_d(z_2) \exp[-K_d(z_1 - z_2)] \quad (8)$$

The contribution of the water column and the bottom to the apparent radiance at the depth z_1 is then modelled using Eqs. (9) and (10) and a least square optimization according to Eq. (6) is performed using L_u instead of R_{rs} .

$$L_u^C(z_1) = \frac{\left\{ r_{rs}^\infty \left(1 - A_o \exp[-(K_d - K_u^C)(H - z_1)] \right) \right\} \cdot \left\{ E_d(z_1) \left(1 - A_o \exp[-K_d(H - z_1)] \right) \right\}}{1 - A_o \exp[-K_u^C(H - z_1)]} \quad (9)$$

$$L_u^B(z_1) = \left\{ E_d(z_2) \exp[-K_d(H - z_2)] A_1 \rho \right\} \exp[-K_u^B(H - z_1)] \quad (10)$$

The Water Colour Simulator (WASI) of Gege (25) was used to estimate the optically active water constituents from *in situ* data. Since only the measured intensity of E_d is used for inversion, there is no influence of the bottom on the recorded signal. WASI allows us to differentiate between direct and diffuse radiation (32) which leads to a highly accurate retrieval of water constituents. Thus, it was used as a validation for the BOMBER inversion results.

APEX data

During the APEX campaign 2011, Lake Starnberg was captured on 10/09/2011 in five stripes (two covering the western shore plus three additional east-west orientated stripes). The data acquisition took place between 11:49 and 12:21 UTC at low solar zenith angles ($43.6^\circ - 45.4^\circ$). The airborne imaging spectrometer APEX (Airborne Prism EXperiment) offers 288 spectral bands covering a wavelength range from 380 – 2500 nm (33). With a field of view of 14° and a flight altitude of 4,900 metres we achieved a spatial resolution of 4 metres. The data was delivered by VITO as level 3A product including geometric and atmospheric correction as well as additional water-air interface correction (i.e. with resulting water-leaving reflectance). For further water analysis, only the first 70 bands were used covering a spectral range from 413 to 745 nm (central wavelengths) and bandwidths (FWHM) between 3.5 and 13.5 nm. Analysis included masking of land and deep water areas as well as inversion using BOMBER to retrieve IOPs and bottom properties with the image analysis software ENVI 4.7 (Exelis).

RESULTS AND DISCUSSION

Inversion of simulated data

The inversion of the simulated data set using the BOMBER implemented algorithms showed very good results regarding the individual *RMSE*, *MAPE* and coefficient of determination (R^2) between input and inversion output for the water constituents (CHL, SPM, cDOM) and the depth (Table 1).

Table 1: Accuracy measures (*RMSE*, *MAPE* and R^2) between input and inversion results of simulated water constituents concentrations and depths and classification accuracies of the bottom coverage (Pixel with 100% coverage of the input bottom).

Bottom albedo input	CHL	SPM	cDOM	Depth	Classification accuracy
white foil	0.068 1.00% 0.998	0.054 0.72% 0.998	0.006 0.16% 0.998	0.653 1.46% 0.982	84%
black foil	0.000 0.00% 1.000	0.000 0.00% 1.000	0.000 0.00% 1.000	0.769 2.05% 0.976	51%
sediment	0.000 0.00% 1.000	0.000 0.00% 1.000	0.000 0.00% 1.000	0.722 2.59% 0.985	73%

root-mean-square error (*RMSE*)

mean absolute percentage error (*MAPE*)

coefficient of determination (R^2)

The high overall agreement between input and output can be explained with the same models used for both calculations and the high spectral resolution of APEX. An artificial error (in percentage of standard deviation) was intentionally omitted, since we were especially interested in the unmixing result of undisturbed spectra (accuracy of correct classification in Table 1). The best classification accuracy of the bottom was obtained over the white foil. However, the water constituents and the depth here showed the highest deviations. This can be explained by the large amount of reflection stemming from the bottom which overframes the water originating part of the reflection and leads to a higher inaccuracy.

The black foil showed low classification accuracy (51%) but a good estimation of water constituents. The *RMSE* and the R^2 -value for the depth showed the worst values for this surface. The classification accuracy over bare sediment is in between the black and the white foil, the water constituents were well retrieved and the depth estimation errors are comparable to the black foil.

The result of the simulated data set showed that the algorithm works best with natural surfaces. This can be explained by the unnatural bright albedo of the white foil compared to natural reflectors (plants, sediment) which were used for the parameterization of Lee et al. (30,31). However, these natural surfaces (especially sediment) have a large spectral variability which causes inaccuracies. Thus, we expect best results for water constituent retrieval above the black foil. The depth estimation will give better results above the white foil.

Inversion of *in situ* data

In a next step, the *in-situ* measured spectra of L_u and E_d were processed using the modified BOMBER algorithm (see above) for three different water depths (3, 6 and 8 m). To provide a large water column which interacts with incident radiation, only the measurements at the uppermost sensor position (sensor depth of 0.5 m) were used for inversion. The measurements at the very shallow littoral terrace (water depth of 0.5 m) were omitted from analysis, since they do not provide a water column large enough for constituent retrieval. The inversion results of L_u (based on Eqs. 7 to 10) for the retrieved water constituents (CHL, SPM and cDOM) and depths from *in situ* RAMSES measurements are shown in Table 2.

Table 2: BOMBER-derived water constituents and water depth (\pm standard deviation σ) from in-situ RAMSES measurements above the white and the black foils at three water depths. The first row shows the real water depth at this position obtained from the attached pressure sensor.

Parameter	Bottom coverage					
	white foil			black foil		
Water depth (real) (m)	8.1	5.6	3.3	8.0	5.5	3.4
Derived water depth $\pm \sigma$ (m)	12.2 \pm 0.4	5.8 \pm 1.8	3.2 \pm 0.1	4.8 \pm 0.2	5.4 \pm 0.7	4.5 \pm 2.2
CHL $\pm \sigma$ (mg m ⁻³)	3.5 \pm 0.2	1.5 \pm 2.1	3.1 \pm 0.7	0.8 \pm 0.1	0.8 \pm 0.1	1.2 \pm 0.4
SPM $\pm \sigma$ (g m ⁻³)	1.7 \pm 0.5	1.4 \pm 0.3	3.2 \pm 0.7	1.4 \pm 0.2	1.5 \pm 0.3	1.7 \pm 0.5
cDOM $\pm \sigma$ (m ⁻¹)	0.4 \pm 0.0	0.4 \pm 0.1	0.4 \pm 0.0	0.4 \pm 0.0	0.4 \pm 0.0	0.5 \pm 0.0

Increasing water depth leads to increasing inaccuracies of the retrieved depth (white foil: overestimation; black foil: underestimation). For the medium (~6 m) and shallow (~3 m) water depths, the inversion above the white foil shows slightly better estimates of the water depth. The derived water constituents show the same values of cDOM absorption with very low standard deviations for all depths and over both foils. The concentrations of SPM and CHL show different values between the black and the white foil with higher mean value variations and standard deviations above the white foil. This is in good agreement with the results from the simulated data set.

To evaluate the BOMBER inversion result of *in situ* measured reflectances (Table 2), the retrieved water constituent concentrations were compared to the WASI-derived concentrations from E_d measurements (Figure 4). The precision of the WASI inversion results was assessed by plotting the sensor depths (measured with an attached pressure sensor) against the depths estimated by WASI. The result (Figure 3) shows a very good agreement between derived and measured sensor depths ($R^2=0.992$).

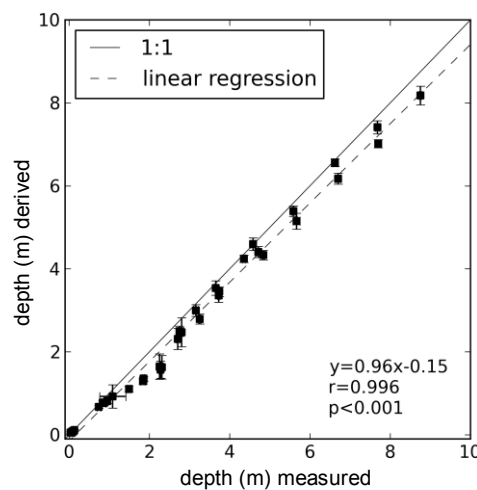


Figure 3: Scatterplot of the WASI-derived sensor depth vs. depth of integrated pressure sensor (mean values of 11 iterations).

All E_d measurements taken under water were processed using WASI. Figure 4 shows the inversion results for the water constituents CHL, SPM and cDOM for the three different water depths. Black squares show the inversion results above the black foil, white squares the results above the white foil.

An increasing concentration can be determined for all IOPs with decreasing sensor depth (please note that always the whole water column above the upward looking sensor is observed). All values have very high standard deviations in the uppermost sensor position (i.e. a water depth of approximately 0.1 m) which can be explained by the very thin water column resulting in large uncertainties of the constituent retrieval. Except for the cDOM concentrations, all depth profiles show the largest value variations at sensor depths between 1 and 2 metres probably due to wave focussing effect at

that depth (34). In general, the WASI-derived concentrations of CHL (1 mg m^{-3}), SPM (2 g m^{-3}) and cDOM (0.5 m^{-1}) correspond to BOMBER-derived inversion results of r_{rs} above the black foil (Table 2).

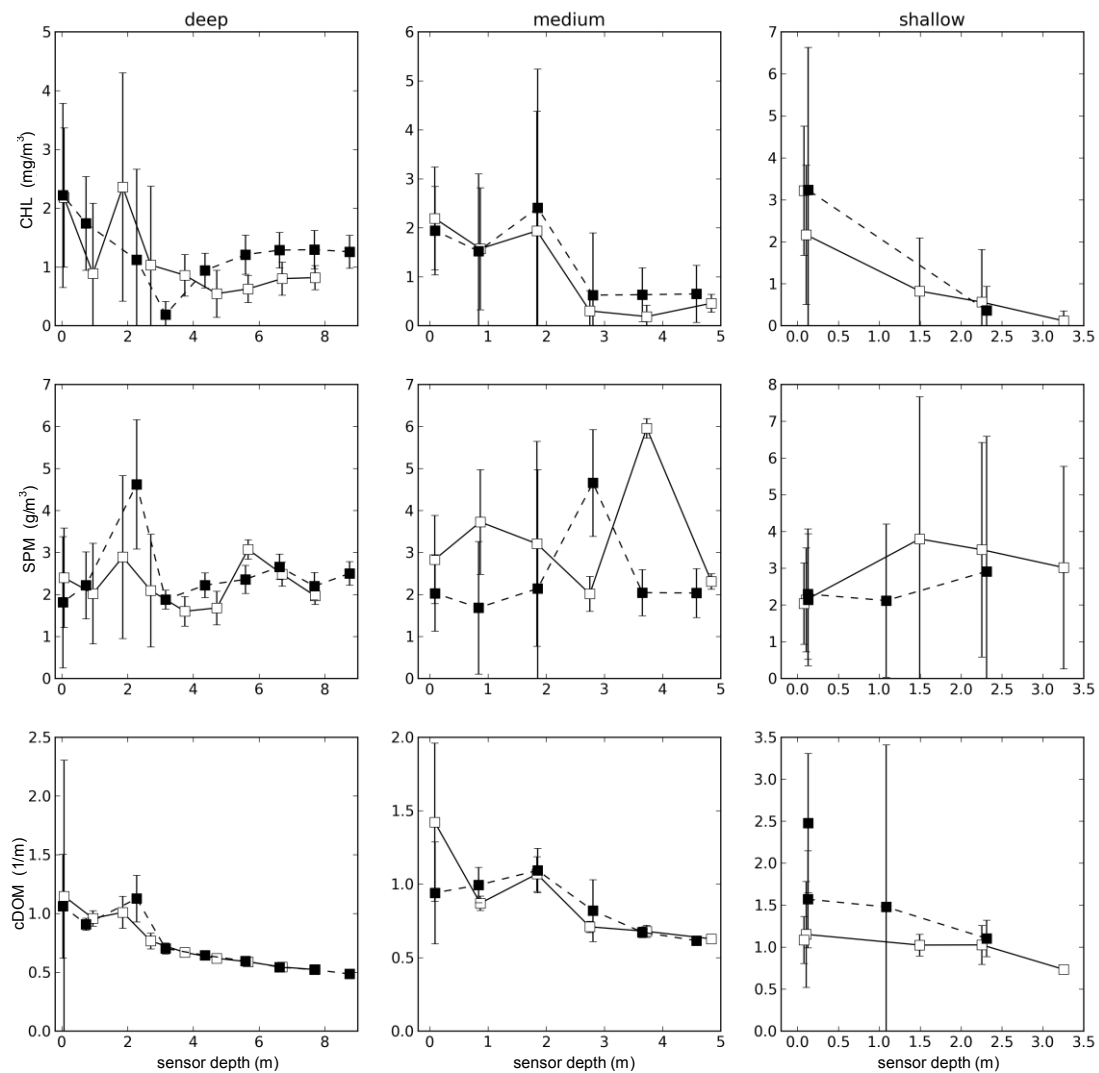


Figure 4: Water constituents derived from WASI inversion of E_d measurements (white squares: above white foil; black square: above black foil), error bars indicate standard deviation of 11 iterated measurements.

BOMBER inversion result of APEX data

The APEX data was delivered atmospherically corrected and additionally corrected for reflection-loss at the water/air interface. The resulting water leaving reflectance (R_w) was further compared to RAMSES measurements above the water surface ($R_{rs}(0+)$). Therefore, pixels representing the foils were manually selected from the APEX image (Figure 5).

For both foils, the APEX-derived reflectances are lower than the in-situ measurements. However, the differences between RAMSES and APEX reflectance account only for 3% at maximum above the white foil (in very shallow water) and up to 1.5% above the black foil. This can be explained by neighbouring effects due to the pixel size of 4 metres and a foil width of only 10 metres which leads to mixed pixels.

The same mask to represent the reflectance above the foils (Figure 5) was used to apply BOMBER to the APEX image only above the foils. Figure 6 shows a map (small subset of the location of the foils) of the BOMBER-derived water constituent concentrations CHL, SPM and cDOM as well as the result of the bottom coverage unmixing result (for the possible endmembers white foil, black foil and bare sediment).

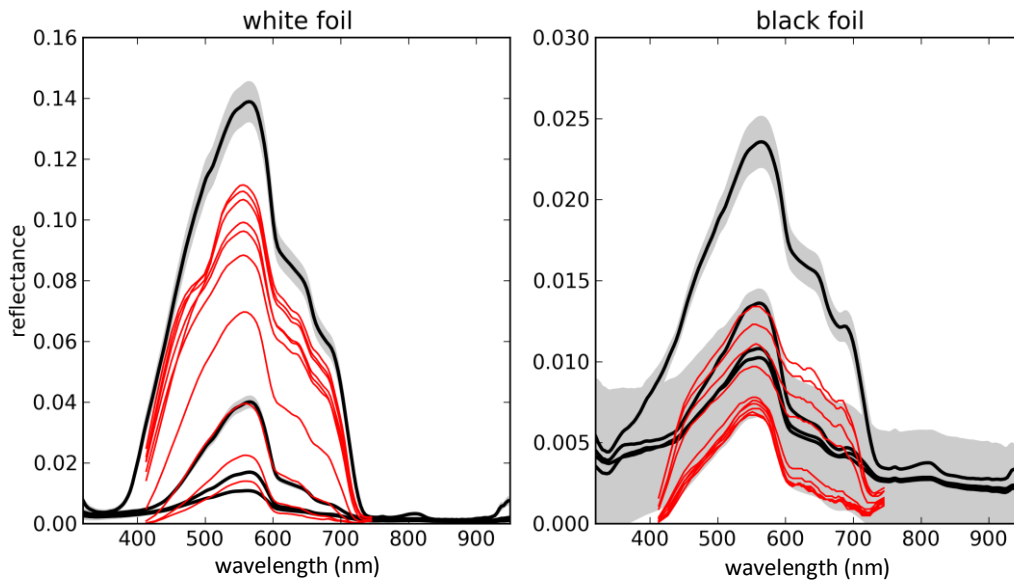


Figure 5: Comparison between APEX-derived reflectances (red) and in-situ measured reflectances (black, grey areas represent the individual standard deviations) above both foils

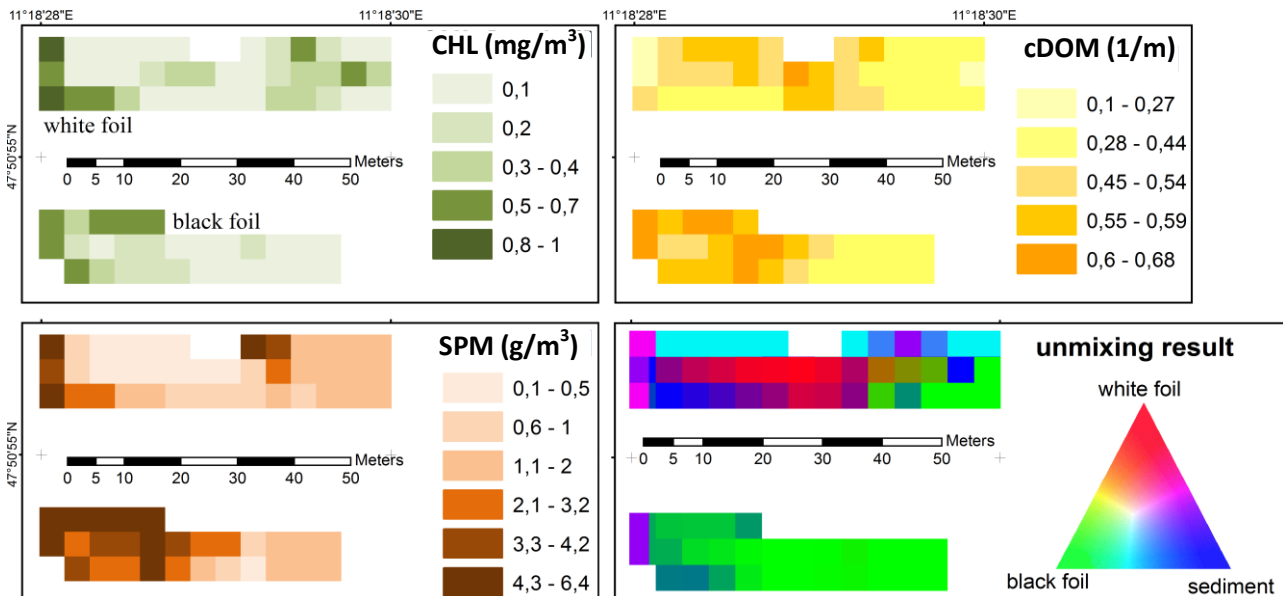


Figure 6: Map showing the BOMBER result for the water constituent concentrations CHL, SPM, cDOM and bottom unmixing for a subset of the APEX image (all areas except for the foils are masked)

The resulting concentrations of cDOM and SPM were best estimated above the black foil agreeing well with the concentrations derived from WASI E_d inversion (Figure 4). CHL was underestimated above both foils. Above the white foil, the water constituent concentrations show larger deviations. This agrees with the inversion results of the simulated data set and the *in situ* reflectance measurements.

In contrast to the simulated data set, the unmixing result of the image data clearly proves that the unnatural bright white foil is not suitable for water constituent retrieval in shallow water with the BOMBER algorithm due to model restrictions. Only a few pixels were completely assigned to that class. As opposed to this, the black foil was also detected at greater water depths and was assigned correctly.

Finally, BOMBER was applied to the whole scene using the same parameterization as defined by Lee et al. (31). The results of IOP retrieval and bottom mapping are shown in Figures 7 and 8.

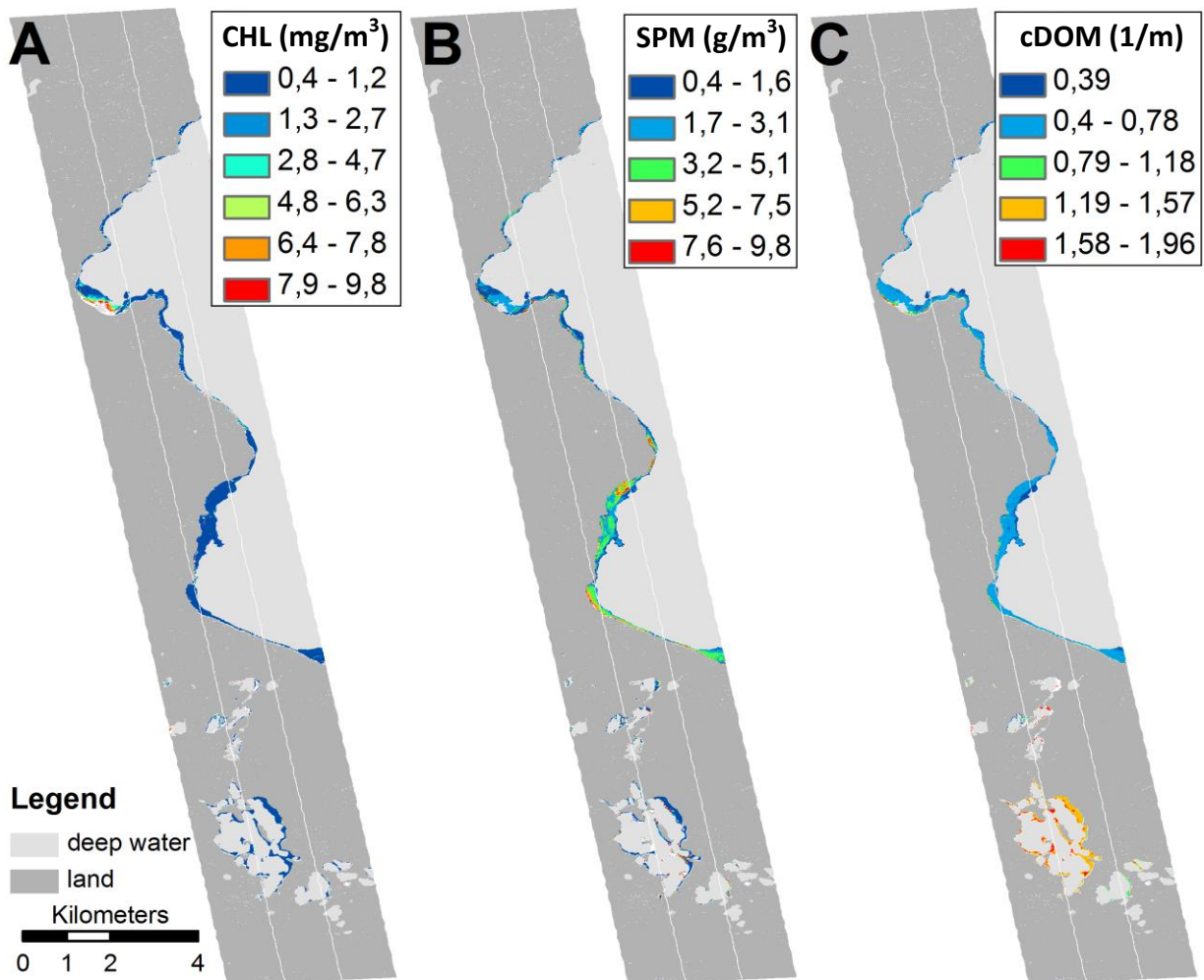


Figure 7: BOMBER-derived concentrations of CHL (A), SPM (B) and cDOM (C) for shallow water of the southern APEX stripe.

The concentration of CHL was generally low at the shallow areas in Lake Starnberg as well as in the adjacent Osterseen lakes in the south, which drain into Lake Starnberg, confirming previous results (21). The SPM concentrations had the highest values in the extended littoral terraces at the south-western edge of the lake. This was probably caused by waves resuspending the fine grained silty sediment in this area. In Lake Starnberg, the content of cDOM was constant, while considerable variations at low spatial scales were found in the Osterseen lakes.

The result of spectral unmixing using the endmember *Najas marina*, *Chara* spp. and uncovered sediment are shown in Figure 8A as well as the estimated water depth (Figure 8B). The RGB composite was created according to the endmember affiliation.

The result for the test site Bernried shows good recognition of *Najas marina* occurring here at a depth range between 2 and 6 metres. The small bay “Karpfenwinkel” at the eastern edge of Lake Starnberg is enlarged, because it is known for a dense coverage of *Characeae* with interspersed *Najas marina*. Here, the endmember *Najas marina* was overestimated, because *Chara* dominates most of the area. However, the non-vegetated areas were very well detected.

Since the concentrations of water constituents at the whole test site Bernried were comparable to the concentrations obtained above the black foil, they can be regarded as valid. Also, the depth was estimated accurately for this particular area, so we assume a reliable determination of BOMBER for these model outputs for the other regions. The misclassification of the region “Karpfenwinkel” might result from ground reflectances different from our test site.

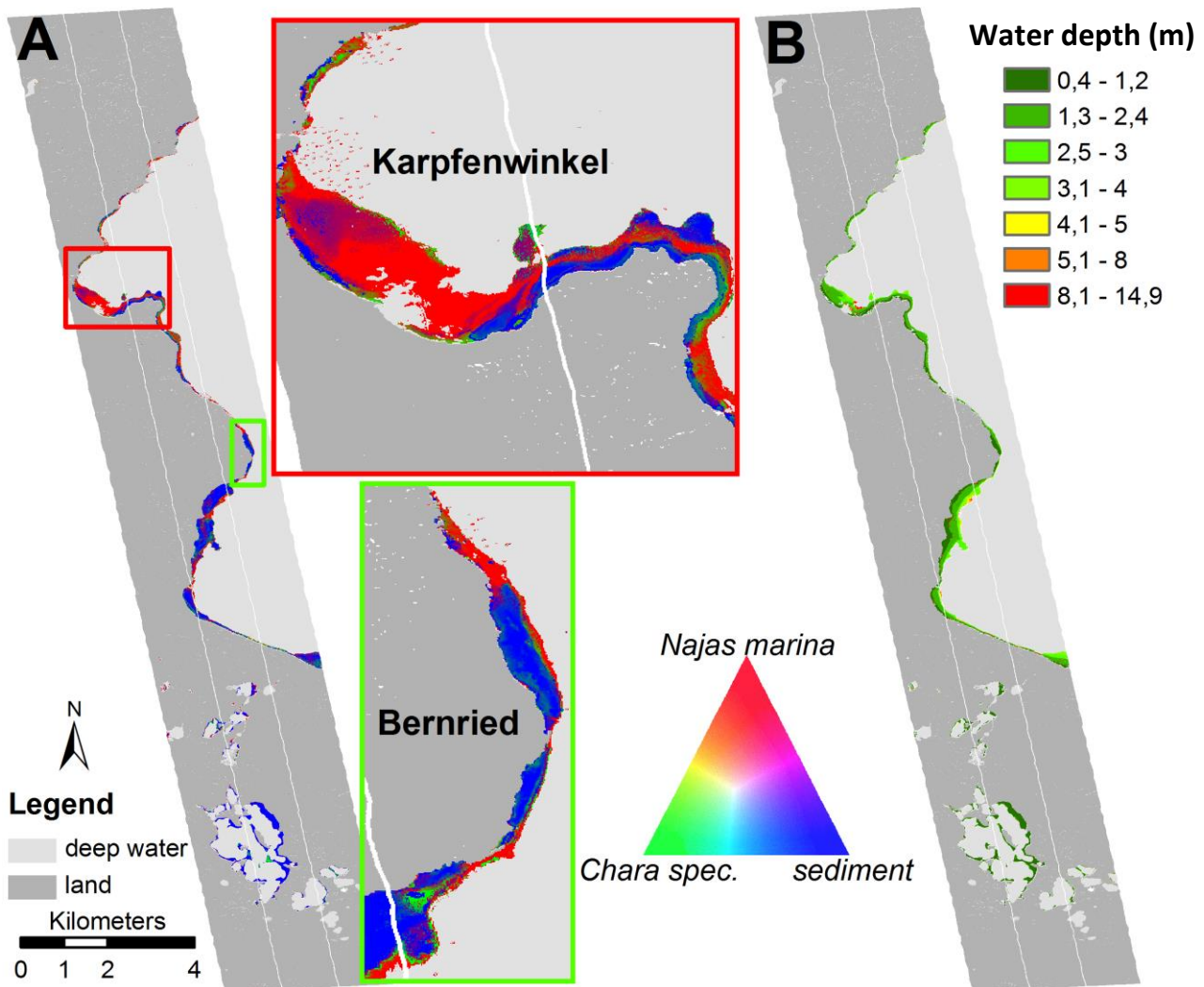


Figure 8: Unmixing result for shallow water bottom coverage (A) and bathymetry (B), zoomed areas show the location of the test site “Bernried” and the bay “Karpfenwinkel”.

CONCLUSIONS

In this work, we showed how submersed artificial surfaces can be used to validate the image-based retrieval of water constituents and depths using the bio-optical model BOMBER. This validation is especially necessary when no reference measurements of water constituents exist and when the depth is unknown.

Based on the results of the simulated data set we showed that measurements above the black foil are better suited for water constituent retrieval using BOMBER. This finding was confirmed by the application of BOMBER to the *in situ* measured reflectances during the APEX flight campaign. The results of BOMBER were validated using measurements of the *in situ* downwelling irradiance which were processed using WASI. The resulting water constituents resembled the ones determined above the black foil. Also, the application of BOMBER to the APEX image data showed that the black foil was properly determined even at greater depths. The retrieved water constituents were comparable to the WASI-derived ones. We expect the classification of the whole scene to be relevant as the water constituents of the test site are of the level as above the black foil.

Based on these results, the application of dark artificial surfaces is a powerful tool when no information on water constituents or bathymetry is available. With dark reference surfaces, “deep water” regions can be created containing water constituent concentrations of shallow water (which often differs from the amount of constituents of the adjacent deep water). The retrieved water con-

stituents and bathymetry above these surfaces (e.g. foils) can be used for the validation of bio-optical model inversion results for the adjacent regions with natural bottom coverage (sediment, vegetation) and enhance the result.

ACKNOWLEDGEMENTS

This project was funded by the Bavarian State Ministry of the Environment and Public Health under the number ZKL01Abt7_18457. Thanks to VITO and the team of the APEX sensor for providing high quality data, to all colleagues from the Limnological Institute who helped during field work and to Claudia Giardino for providing the software BOMBER. Special thanks to the two anonymous reviewers for their helpful comments and to Katrin Zwirgmaier for improving our English.

REFERENCES

- 1 Mobley C D, 1994. Light and Water (Academic Press) 592 pp.
- 2 Gordon H R, O B Brown & M M Jacobs, 1975. Computed relationships between the inherent and apparent optical properties of a flat homogeneous ocean. Applied Optics, 14(2): 417-427
- 3 Kirk J T O, 1984. Dependence of relationship between inherent and apparent optical properties of water on solar altitude. Limnology and Oceanography, 29(2): 350-356
- 4 Morel A & B Gentili, 1993. Diffuse reflectance of oceanic waters. II. Bidirectional aspects. Applied Optics, 32(33): 6864-6879
- 5 Albert A & C Mobley, 2003. An analytical model for subsurface irradiance and remote sensing reflectance in deep and shallow case-2 waters. Optics Express, 11(22): 2873-2890
- 6 Morel A, 1980. In-water and remote measurements of ocean color. Boundary-Layer Meteorology, 18(2): 177-201
- 7 Gordon H R & M Wang, 1994. Retrieval of water-leaving radiance and aerosol optical thickness over the oceans with SeaWiFS: a preliminary algorithm. Applied Optics, 33(3): 443-452
- 8 Gordon H R & D K Clark, 1981. Clear water radiances for atmospheric correction of coastal zone color scanner imagery. Applied Optics, 20(24): 4175-4180
- 9 Kallio K, J Pulliainen & P Ylöstalo, 2005. [MERIS, MODIS and ETM+ channel configurations in the estimation of lake water quality from subsurface using semi-analytical and empirical algorithms.](#) Geophysica, 41(1-2): 31-55
- 10 Carder K L, F R Chen, J P Cannizzaro, J W Campbell & B G Mitchell, 2004. Performance of the MODIS semi-analytical ocean color algorithm for chlorophyll-a. Advances in Space Research, 33(7): 1152-1159
- 11 Doxaran D, P Castaing & S J Lavender, 2006. Monitoring the maximum turbidity zone and detecting fine-scale turbidity features in the Gironde estuary using high spatial resolution satellite sensor (SPOT HRV, Landsat ETM+) data. International Journal of Remote Sensing, 27(11): 2303-2321
- 12 Odermatt D, A Gitelson, V E Brando & M Schaepman, 2012. Review of constituent retrieval in optically deep and complex waters from satellite imagery. Remote Sensing of Environment, 118(0): 116-126
- 13 Kallio K, T Kutser, T Hannonen, S Koponen, J Pulliainen, J Vepsäläinen & T Pyhälähti, 2001. Retrieval of water quality from airborne imaging spectrometry of various lake types in different seasons. Science of The Total Environment, 268(1-3): 59-77
- 14 Koponen S, J Pulliainen, K Kallio & M Hallikainen, 2002. Lake water quality classification with airborne hyperspectral spectrometer and simulated MERIS data. Remote Sensing of Environment, 79(1): 51-59

- 15 Thiemann S & H Kaufmann, 2002. Lake water quality monitoring using hyperspectral airborne data - a semiempirical multisensor and multitemporal approach for the Mecklenburg Lake District, Germany. Remote Sensing of Environment, 81(2-3): 228-237
- 16 Van Stokkom H T C, G N M Stokman & J W Hovenier, 1993. Quantitative use of passive optical remote sensing over coastal and inland water bodies. International Journal of Remote Sensing, 14(3): 541-563
- 17 Hakvoort H, J de Haan, R Jordans, R Vos, S Peters & M Rijkeboer, 2002. Towards airborne remote sensing of water quality in The Netherlands - validation and error analysis. ISPRS Journal of Photogrammetry and Remote Sensing, 57(3): 171-183
- 18 Albert A, 2004. [Inversion Technique for Optical Remote Sensing in Shallow Water](#). PhD Thesis, Universität Hamburg, 188 pp.
- 19 Hooker S B, G Zibordi, J-F Berthon & J W Brown, 2004. Above-water radiometry in shallow coastal waters. Applied Optics, 43(21): 4254-4268
- 20 Heege T, A Bogner & N Pinnel, 2003. Mapping of submerged aquatic vegetation with a physically based processing chain. In: SPIE - The International Society for Optical Engineering, edited by E. Kramer (SPIE, Barcelona), 43-50
- 21 Pinnel N, 2007. [A method for mapping submerged macrophytes in lakes using hyperspectral remote sensing](#). PhD Thesis, Technische Universität München, 164 pp. (last date accessed: 8 May 2013)
- 22 Gullström M, B Lundén, M Bodin, J Kangwe, M C Öhman, M S P Mtolera & M Björk, 2006. Assessment of changes in the seagrass-dominated submerged vegetation of tropical Chwaka Bay (Zanzibar) using satellite remote sensing. Estuarine, Coastal and Shelf Science, 67(3): 399-408
- 23 Lu D & H J Cho, 2010. An improved water-depth correction algorithm for seagrass mapping using hyperspectral data. Remote Sensing Letters, 2(2): 91-97
- 24 McIntyre M, D Naar, K Carder, B Donahue & D Mallinson, 2006. Coastal bathymetry from hyperspectral remote sensing data: comparisons with high resolution multibeam bathymetry. Marine Geophysical Research, 27(2): 129-136
- 25 Gege P, 2004. The water color simulator WASI: an integrating software tool for analysis and simulation of optical in situ spectra. Computers & Geosciences, 30(5): 523-532
- 26 Giardino C, G Candiani, M Bresciani, Z Lee, S Gagliano & M Pepe, 2012. BOMBER: A tool for estimating water quality and bottom properties from remote sensing images. Computers & Geosciences, 45: 313-318
- 27 Tolk B L, L Han & D C Rundquist, 2000. The impact of bottom brightness on spectral reflectance of suspended sediments. International Journal of Remote Sensing, 21(11): 2259-2268
- 28 Cho H J & D Lu, 2010. A water-depth correction algorithm for submerged vegetation spectra. Remote Sensing Letters, 1(1): 29-35
- 29 Fesq-Martin M, A Lang & M Peters, 2008. Der Starnberger See - Natur- und Vorgeschichte einer bayerischen Landschaft (Pfeil-Verlag) 145 pp.
- 30 Lee Z, K L Carder, C D Mobley, R G Steward & J S Patch, 1998. Hyperspectral remote sensing for shallow waters. I. A semianalytical model. Applied Optics, 37(27): 6329-6338
- 31 Lee Z, K L Carder, C D Mobley, R G Steward & J S Patch, 1999. Hyperspectral remote sensing for shallow waters. 2. Deriving bottom depths and water properties by optimization. Applied Optics, 38(18): 3831-3843
- 32 Gege P, 2012. Estimation of phytoplankton concentration from downwelling irradiance measurements in water. Israel Journal of Plant Sciences, 60(1-2): 193-207

- 33 Itten K, et al., 2008. [APEX - the Hyperspectral ESA Airborne Prism Experiment](#). Sensors, 8(10): 6235-6259
- 34 Gege P & N Pinnel, 2011. Sources of variance of downwelling irradiance in water. Applied Optics, 50(15): 2192-2203